ORIGINAL PAPER

A Study of the Morlogical Properties of $SrFe_{12-x}Co_xO_{19}$ (x = 0, 0.1, 0.2) Hexaferrite Nanoparticles

M. Zargar Shoushtari · S. E. Mousavi Ghahfarokhi · F. Ranjbar

Abstract In this work, a series of M-type strontium hexaferrite samples having nominal composition $SrFe_{12-x}Co_xO_{19}$ (x = 0.0, 0.1 and 0.2) with different morphologies have been synthesized by sol-gel method The decomposition behavior and mechanism of phase formation of $SrFe_{12}O_{19}$ were investigated using of thermogravimetric analysis (DTA/TGA). The crystal structure and morphology of samples were characterized by X-ray diffraction (XRD) and scanning electron microscopy (SEM), respectively. The XRD results showed that all of the samples have the major phase of $SrFe_{12}O_{19}$ with M-type hexaferrite structure, and the Co-doped samples also have the minor phases of Fe_2O_3 and $K_2Fe_{10}O_{16}$. It seems that the Fe^{3+} ions are substituted by Co^{2+} ions in the crystallography sites of the $SrFe_{12}O_{19}$ structure. The average crystallites size is found in the range of 16-39 nm, which is small enough to obtain a suitable signal-to-noise ratio in high-density recording media. The morphology and average particles size of samples were determined by SEM. In the Fourier transform infrared spectrometry (FT-IR) spectra of all the samples, three peaks were observed. All of these peaks correspond to the metal-oxygen stretching in hexaferrites.

1 Introduction

Ferrites are ferrimagnetic ceramic materials that can be magnetized to produce large magnetic flux densities in response to small applied magnetic forces [1]. M-type hexagonal hard ferrites, $MFe_{12}O_{19}$, (where M is Ba, Sr, or Pb), have attracted extensive interests since their discovery in 1950s, due to their applications in permanent magnets, microwave devices, and high-density magnetic recording media, particularly in perpendicular magnetic recording [2]. The unit cell ($MFe_{12}O_{19}$) of the hexaferrite system contains two formula units consisting of ten hexagonally closed-packed oxygen layers stacked along the hexagonal basal plane (c-axis). The divalent ion, M^{2+}, is substituted for an oxygen atom in every fifth layer. The Fe^{3+} ions are distributed on five different crystallographic sites: three octahedral (12k, 2a and $4f_2$), one tetrahedral ($4f_1$) and one trigonal bipyramidal (2b). In $MFe_{12}O_{19}$, 8 of the 12 Fe^{3+} ions at 12k, 2a and 2b lattice sites have upward spin (↑), while the remaining 4 ions at $4f_1$ and $4f_2$ sites have downward spin (↓) [3]. For improvement of various properties of strontium hexaferrites, the substitution of several cations such as Cr^{3+}, Al^{3+} [4], Zn^{2+}, Co^{2+}, and Ni^{2+} [5] and cations combinations such as La^{3+}–Co^{2+}, Ti^{4+}–Co^{2+} [4], Al^{3+}–Ga^{3+} and Zr^{4+}–Ni^{2+} [6] on the Fe^{3+} site of hexaferrites have been investigated and discussed. Many attempts have been developed to modify the properties of ferrites among which one is to use inorganic ions because of their ability for selective growth of the samples in particular direction [7]. Studies have been carried out to determine the influence of various template agents on the morphology

M. Zargar Shoushtari · S. E. Mousavi Ghahfarokhi (✉) · F. Ranjbar
Department of Physics, Shahid Chamran University of Ahvaz, Ahvaz, Islamic Republic of Iran
e-mail: mousavi355@scu.ac.ir

M. Zargar Shoushtari
e-mail: zargar@scu.ac.ir

F. Ranjbar
e-mail: Ranjbar.8814709@yahoo.com

of strontium ferrites. Yongfei et al. [8] have studied the influence of inorganic template agents (KCl, KBr, and KI) on the morphology of the $SrFe_{12}O_{19}$ nanoparticles and have reported that the addition of KCl, KBr, and KI lead to the formation of needle-like, rod-like, and spherical $SrFe_{12}O_{19}$, respectively. The properties of strontium ferrites can be improved by changing its microstructure, chemical composition, size, and morphology [2]. Several methods have been developed to synthesize nanoparticles of strontium hexaferrite, such as the coprecipitation, glass crystallization, self-propagating high-temperature synthesis, and the sol–gel methods [9]. The preparation technology of fine $SrFe_{12}O_{19}$ with different morphology using sol–gel method has been done in reference [8], but the preparation of $SrFe_{12-x}Co_sO_{19}$ with different morphology especially sol–gel method has not yet been reported. In the present investigation, the doped $SrFe_{12-x}Co_xO_{19}$ ($x = 0.1$ and 0.2) and undoped $SrFe_{12}O_{19}$ hexaferrites have been synthesized. The influence of inorganic template agents (KCl, KBr, and KI) on the undoped and Co-doped samples and their structure as well as their morphology and also the role of Co have been studied.

2 Materials and Methods

In order to synthesize $SrFe_{12-x}Co_xO_{19}$ nanoparticles (where $x = 0.0$, 0.1 and 0.2) with different morphologies, the stoichiometric amounts of $Fe(NO_3)_3 \cdot 9H_2O$, $Sr(NO_3)_2$, and $Co(NO_3)_3 \cdot 6H_2O$ were dissolved in deionized water. Then, the entire mixture was stirred in water bath at 80 °C until $Fe(NO_3)_3 \cdot 9H_2O$, $Sr(NO_3)_2$, and $Co(NO_3)_3 \cdot 6H_2O$ were completely dissolved. After that, the citric acid was added to the above solution according to the molar ratio 1:1 to Sr^{2+}. The pH value of the solution was adjusted to 6 with $NH_3 \cdot H_2O$. This solution was evaporated until the gel was formed; then, this gel was dried at 90 °C to obtain a dry gel. The KCl, KBr, and KI were respectively mixed into dry gel according to the mass ratio of dry gel to salt of 1:3. The mixture of salt and dry gel was calcined at 1000 °C for 2 h. The calcined ferrite was washed with distilled water until deposition did not appear when adding $AgNO_3$ in the lotion; the pure $SrFe_{12-x}Co_xO_{19}$ with different morphologies was prepared after centrifugalization and drying process. The spherical $SrFe_{12}O_{19}$ nanoparticles were prepared only by calcined dry gel. The thermal behavior of the dry gel precursor sample was evaluated by simultaneous thermogravimetric analysis/differential thermal analysis (TGA/DTA) (STA 503/Bahr2010). The X-ray diffraction (Philips PW-1840) was used for phase analysis. The Fourier transform infrared spectrometry (FT-IR) (BOMEN/MB102) in the range 400–4000 cm^{-1} was performed on powder. The scanning electron microscopy (S-4160/Hitachi) was also used to determine the morphology and size of the particles. The structural properties of the samples such as lattice parameters a and c (1), ratio of c/a, cell volume (2), percent phases obtained, and average crystallites size (3) were calculated from X-ray diffraction (XRD) patterns [10].

$$\frac{1}{d_{hkl}^2} = \frac{4}{3}\left(\frac{h^2 + hk + k^2}{a^2}\right) + \frac{l^2}{c^2} \tag{1}$$

$$V_{cell} = 0.8666a^2c \tag{2}$$

$$D = \frac{0.89\lambda}{\beta\cos\theta} \tag{3}$$

Where a and c are lattice constants, V_{cell} is the unit cell volume, λ is the X-ray wavelength, β is the half-peak width, and θ is the Bragg angle.

3 Results and Discussion

Figure 1 shows the thermogravimetric analysis (TG) and differential thermal analysis (DTA) curve of the dry gel precursor of $SrFe_{12}O_{19}$ hexaferrite. During heat treatment of
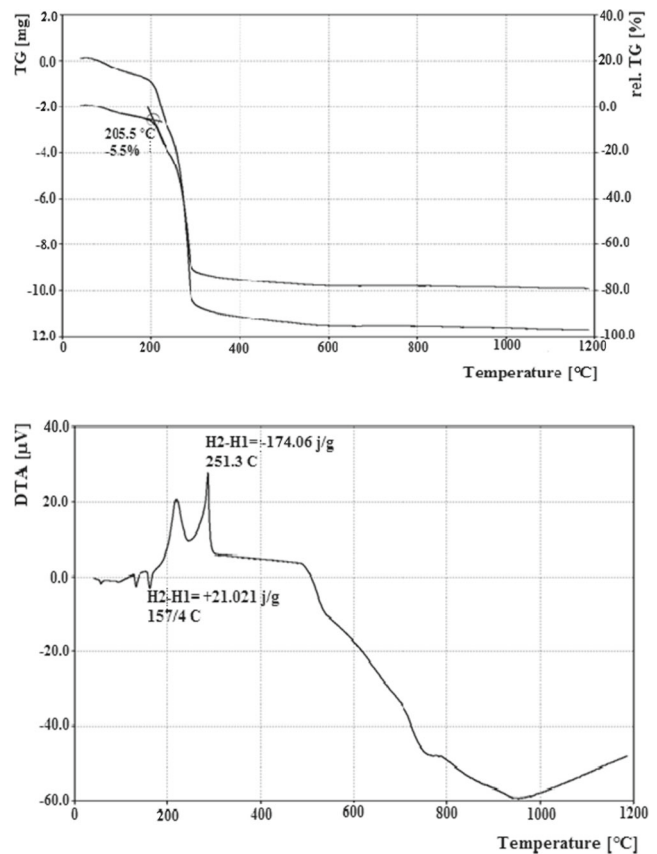
Fig. 1 Thermo–gravimetric (TG) curve and differential thermal analysis (DTA) curve of the dry–gel precursor of the $SrFe_{12}O_{19}$ hexaferrite

the samples, several processes such as dehydration, decomposition, and sintering take place [11]. The TG curve reveals four distinct steps of weight loss. The first weight loss step (5.5 %) over the temperature range from room temperature to about 205.5 °C is due to the loss of residual water in the dry gel precursor. The second weight loss from 205.5 to 300 °C is due to the burning of citric acid and the complete decomposition of the organic material. The third weight loss from 300 to 600 °C is attributed to the formation of intermediate hematite (α-Fe_2O_3) phase. The weight of the sample remains constant between 600 and 850 °C, and there is no noticeable weight loss, but according to the XRD results, the strontium hexaferrite phase is started in this range of temperatures. The small weight loss in temperatures of more than 850 °C could be due to the removed of α-Fe_2O_3 impurity phase and formation single-phase strontium hexaferrite. It is believed that the M-type hexagonal phase formation begins at $\sim$ 700 °C but still contains α-Fe_2O_3 impurity phase which is completely removed at calcination temperature of 1000 °C.

The thermo-chemical behavior was consistent with that described by the DTA curve; the DTA pattern also complements the abovementioned observations (Fig. 1). The DTA curve shows six endothermic peaks around 60, 140, 157.4, 225, 780, and 940 °C and three exothermic peaks around 205.5, 251.3, and 790 °C. The first three endothermic peak are due to the vaporization of any adsorbed water; the endothermic peak at 225 °C, between two exothermic peaks 205.5 and 251.3 °C, was ascribed to the combustion of the uncompleted citric acid and the complete decomposition of the organic material; the endothermic peak at 780 °C

indicates that the endothermic reaction result in the formation of and $SrFe_{12}O_{19}$. The endothermic peak around 940 °C indicates the endothermic reaction result in the formation of pure $SrFe_{12}O_{19}$ which is also confirmed by the XRD analysis of the residue after the DTA analysis at 1000 °C (Fig. 2). The first exothermic peak around of 205.5 °C may be attributed to the evaporation of the residual nitrate and organic matter, and the second exothermic peak around 251.3 °C could be referred to the formation of α-Fe_2O_3 and a phase transition, that is, the formation of strontium ferrite. The third exothermic peak around 790 °C indicates the formation of strontium ferrite.

Figures 2, 3, and 4 show the XRD patterns of $SrFe_{12-x}Co_xO_{19}$ ($x = 0.0$, 0.1 and 0.2) hexaferrites prepared by adding inorganic template agent (KCl, KBr, and KI). The XRD results revealed that all of the samples of $SrFe_{12-x}Co_xO_{19}$ ($x = 0.0$, 0.1 and 0.2) without the inorganic template agents have M-type hexaferrite structure. It seems that the Fe^{3+} ions are substituted by Co^{2+} ions in the crystallography sites of the $SrFe_{12}O_{19}$ structure.

The diffraction peaks at 2θ values of 32.352°, 34.183°, 56.852°, and 63.132° corresponded to the strongest diffraction planes (1 0 7), (1 1 4), (2 0 11), and (2 2 0), respectively. These patterns ascribed to M-type strontium hexaferrite phase. Moreover, the diffraction peaks at 2θ values of 33.153° and 54.091° reflected the presence of α-Fe_2O_3 phase. All of the reflections were indexed on the basis of the M-type structure retaining the $P6_3/mmc$ space group, with the initial cell parameters of $a = 5.886$ Å and $c = 23.037$ Å, and the JCPDS card number (33–1340) had been referred to all the peak position identification.

Fig. 2 XRD patterns of the $SrFe_{12}O_{19}$ samples: **a** blank, **b** KCl, **c** KBr, and **d** KI
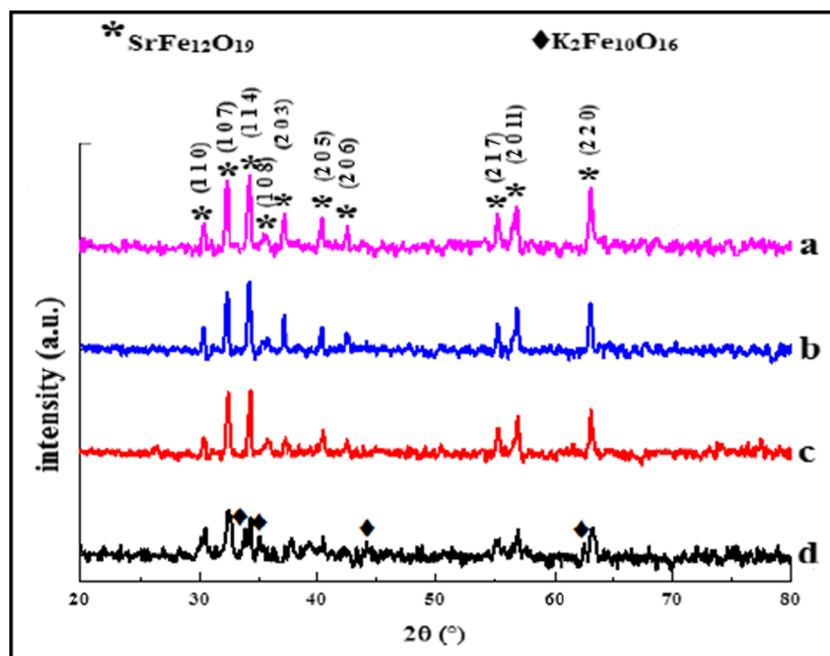
**Fig. 3** XRD patterns of the SrFe$_{11.9}$Co$_{0.1}$O$_{19}$ samples: **a** blank, **b** KCl, **c** KBr, and **d** KI
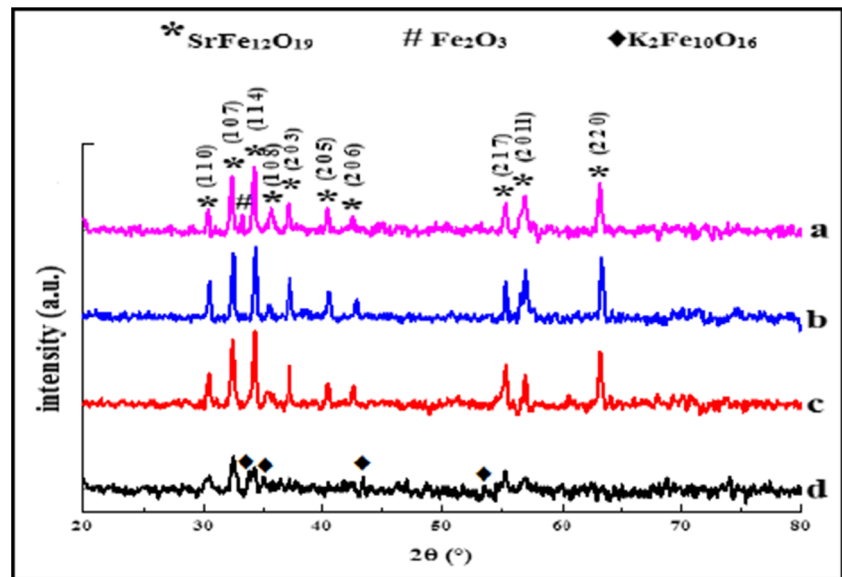
Compared with the JCPDF card (code 33-1340) standard XRD pattern, we can come to a conclusion: some peaks associated with α-Fe$_2$O$_3$ and spinel-type structure SrFe$_2$O$_4$ phases were not found in the XRD patterns of powder prepared by adding KCl and KBr. The XRD patterns indicate that the crystal structure of the ferrite samples does not transform and remains magnetoplumbite on the addition of inorganic template agents KCl and KBr. In the X-ray diffractographs for all the samples obtained with KI, an extra peak corresponding to the formation of K$_2$Fe$_{10}$O$_{16}$

secondary phase is observed. Since the calcination temperature of samples is 1000 °C and melting point of KI is 681 °C, the formation of K$_2$Fe$_{10}$O$_{16}$ phase can be explained on the basis of that KI with calcination gets oxidized, which plays a critical role in the formation of K$_2$Fe$_{10}$O$_{16}$ phase in the sample prepared by adding KI [7]. Therefore, reduction of the calcination temperature of samples removed the K$_2$Fe$_{10}$O$_{16}$ additional phase (Yongfei et al. [8]).

The lattice parameters a and c, ratio of c/a, cell volume (V), percent phases obtained, and average crystallites

Fig. 4 XRD patterns of the SrFe$_{11.8}$Co$_{0.2}$O$_{19}$ samples: **a** blank, **b** KCl, **c** KBr, and **d** KI
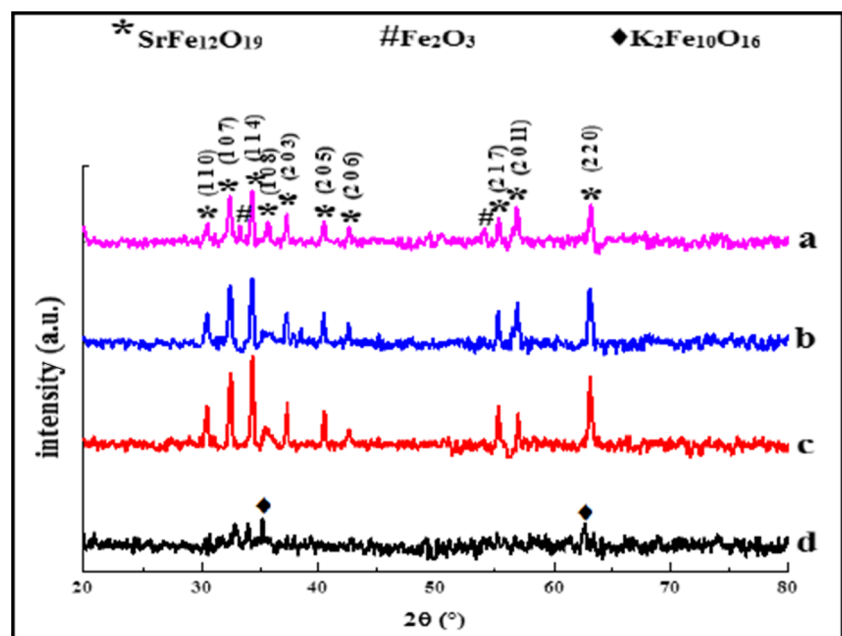
Table 1 The lattice parameters a(Å) and c (Å), ratio of c/a, cell volume (Å^3), percent phases obtained, average crystallites size (nm), and average particles size of the SrFe$_{12-x}$Co$_x$O$_{19}$ ($x = 0.0$, 0.1, and 0.2) with different morphologies ("–" is not calculated)

| x	Dopant	Morphology	a(Å)	c(Å)	Ratio of $\frac{*}{*}$	Cell volume (Å^3)	% Phases obtained	Average crystallites size (nm)	Average particles size (nm)
0	Blank	Spherical	5.883	23.159	3.936	694.587	100 % SrFe$_{12}$O$_{19}$	25.72	34.46
0	KCl	Needle-like	5.881	23.106	3.929	692.541	100 % SrFe$_{12}$O$_{19}$	29.86	78.10
0	KBr	Hexagonal plates	5.886	23.003	3.908	690.627	100 % SrFe$_{12}$O$_{19}$	29.21	79.56
0	KI	Hexagonal plates	5.864	23.054	3.931	686.994	63.39 % SrFe$_{12}$O$_{19}$ 36.61 % K$_2$Fe$_{10}$O$_{16}$	16.32	72.22
0.1	Blank	Flower	5.906	23.089	3.909	697.928	93.40 % SrFe$_{12}$O$_{19}$ 6.60 % Fe$_2$O$_3$	28.77	27.18
0.1	KCl	Thin hexagonal plates	5.887	22.942	3.897	689.030	100 % SrFe$_{12}$O$_{19}$	32.55	47.85
0.1	KBr	—-	5.886	23.008	3.909	690.777	100 % SrFe$_{12}$O$_{19}$	28.78	—-
0.1	KI	—-	5.860	23.151	3.951	688.944	69.77 % SrFe$_{12}$O$_{19}$ 30.23 % K$_2$Fe$_{10}$O$_{16}$	19.37	—-
0.2	Blank	—-	5.886	23.008	3.909	690.777	93.96 % SrFe$_{12}$O$_{19}$ 6.03 % Fe$_2$O$_2$	30.26	—-
0.2	KCl	Skein-like	5.886	23.008	3.909	690.777	100 % SrFe$_{12}$O$_{19}$	26.30	26.83
0.2	KBr	Thin hexagonal plates	5.893	22.904	3.887	689.291	100% SrFe$_{12}$O$_{19}$	31.30	66.92
0.2	KI	Sponge-like	5.892	23.255	3.947	699.617	69.63% SrFe$_{12}$O$_{19}$ 30.37% K$_2$Fe$_{10}$O$_{16}$	39.86	22.93

size (D) were calculated from XRD patterns are given in Table 1. According to Verstegen and Stevels, an examination of c/a parameter ratio may be used to quantify the structure type, as the M-type structure can be assumed if the ratio is observed to be less than 3.98 [12]. As shown in Table 1, the c/a ratios were calculated for the samples, ranged from 3.887 to 3.951; therefore our samples have an M-type structure.

Figure 5 shows the FT-IR spectra of the SrFe$_{12-x}$Co$_x$O$_{19}$ ($x = 0$) hexaferrites prepared by adding inorganic template agent (KCl, KBr, and KI). In the FT-IR spectra of all the samples, the frequency bands in the range 550–580 and 430–470 cm^{-1} correspond to the formation of tetrahedral and octahedral clusters, respectively, which confirms the presence of metal–oxygen stretching band in ferrites. The vibrational mode of tetrahedral clusters is higher as compared to that of octahedral clusters, which is due to the shorter bond length of tetrahedral clusters [7]. The frequency bands at 849.088 and 926.328 cm^{-1} in the sample with KI is attributed to the K$_2$Fe$_{10}$O$_{16}$

secondary phase. Thus, the results of FT-IR spectra are in a good agreement with the TGA/DTA and XRD data.

The structural morphology of SrFe$_{12-x}$Co$_x$O$_{19}$ ($x = 0.0$, 0.1 and 0.2) hexaferrites prepared by adding inorganic template agent (KCl, KBr, and KI) was studied by scanning electron microscopy (SEM), and it is given in Figs. 6, 7, and 8. When the nanoferrite samples have been incorporated with the inorganic ions (KCl, KBr, and KI), the morphology of the nanoferrite samples gets modified according to the shielding ability of the ions [7]. Figure 6a represents the typical SEM images of SrFe$_{12}$O$_{19}$ without inorganic template agent. It can be seen that the samples prepared by adding KCl have needle-like morphology, while those prepared by adding KBr and KI have a hexagonal plate-like structure. This may be attributed to the fact that the growth of the crystal takes place in different orientations in the presence of KCl, KBr, and KI. This is because at high temperature, the inorganic molecule forms a partial liquid phase at the grain boundaries and is captured by the surface of the crystal followed by its transfer in the crystal face. The ability of

**Fig. 5** FT–IR spectra of the $SrFe_{12}O_{19}$ samples: **a** blank, **b** KCl, **c** KBr, and **d** KI
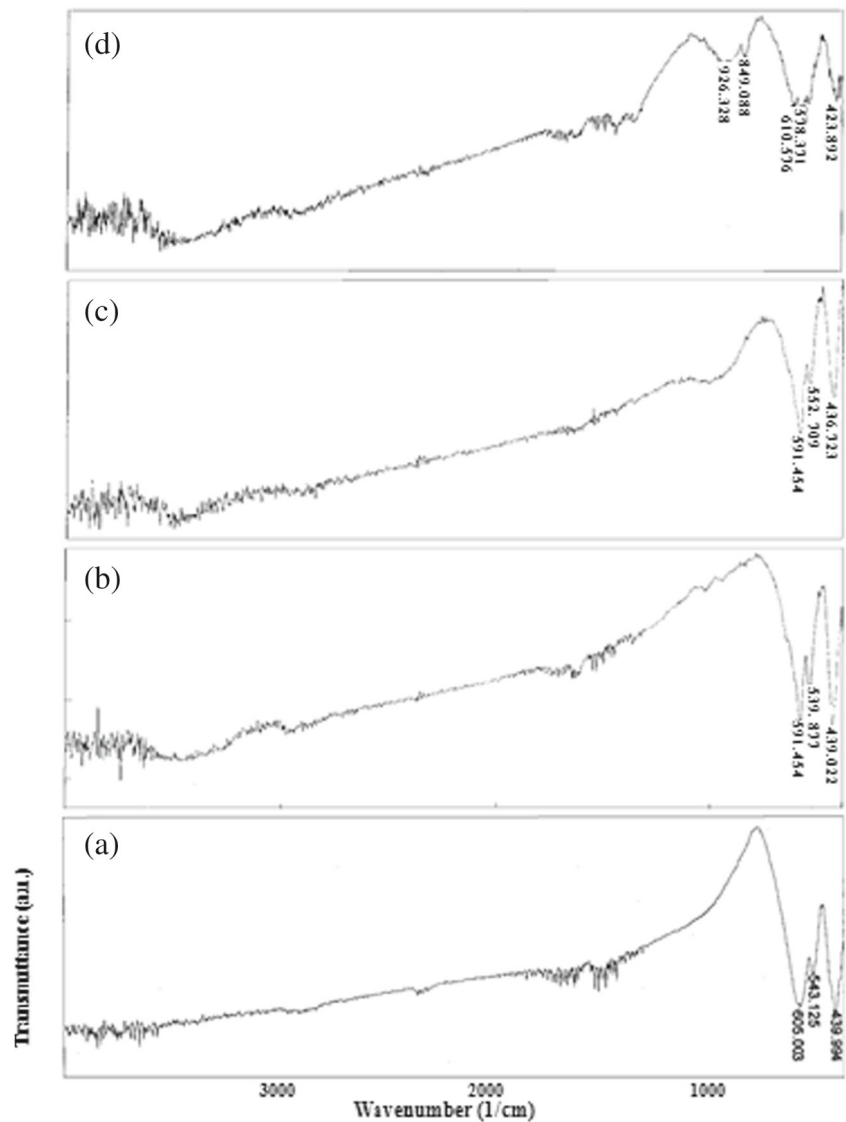
the molecule to get absorbed in the crystal face depends on the coordination ability of the anion, which in turn affects the orientation of the growth of the crystal [2]. Cl^- being smaller in size has higher coordination ability. It shields the crystal along the faces to which it gets coordinated and therefore allows the growth of the crystal only in one dimension leading to a needle-like morphology. Br^- is larger in size; therefore, it has a lower charge: size ratio as compared to Cl^- due to which its coordination ability is lower than that of Cl^-. Hence, it shields the crystal only along one dimension and allows its growth in two dimensions resulting in hexagonal plate-like structure.

KI is easily oxidized to $K_2Fe_{10}O_{16}$ which sublimes at high temperature and is entrapped in the ferrite crystal causing growth of crystal in two dimensions, which results in a hexagonal plate-like morphology. It means that the morphology anisotropy of the samples gets increased with

incorporation of KCl, KBr, and KI. The platelets have different thickness depending on the ability of the ions to deactivate various phases of hexaferrites [7]. It is reported that strontium hexaferrite nanoparticles with hexagonal plate-like morphology are potential materials for the RADAR absorption applications [13]. Hence, morphology of the sample can be easily tuned according to the research interest by incorporating with inorganic template agent. The morphology and average particles size of samples were determined from SEM are given in Table 1.
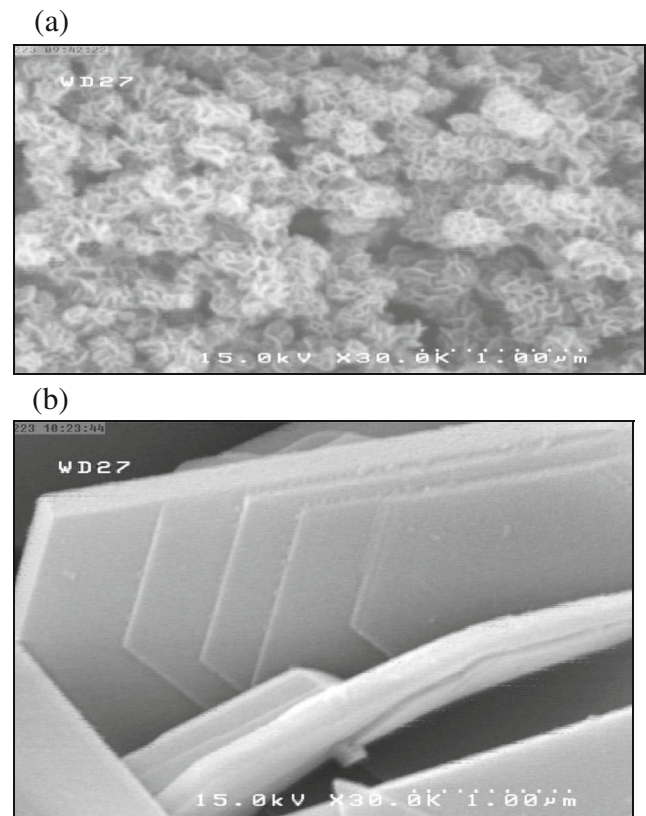
The morphology of samples prepared by adding KCl, KBr, and KI has enormous change, compared with those without inorganic template agent added in the process of calcination. The calcination process contains the decomposition of citric acid, the crystallization of product, the formation of microcrystal, the gradual growth, and perfection of crystal. The morphology of crystal is determined by

(a)

(b)

(c)

(d)
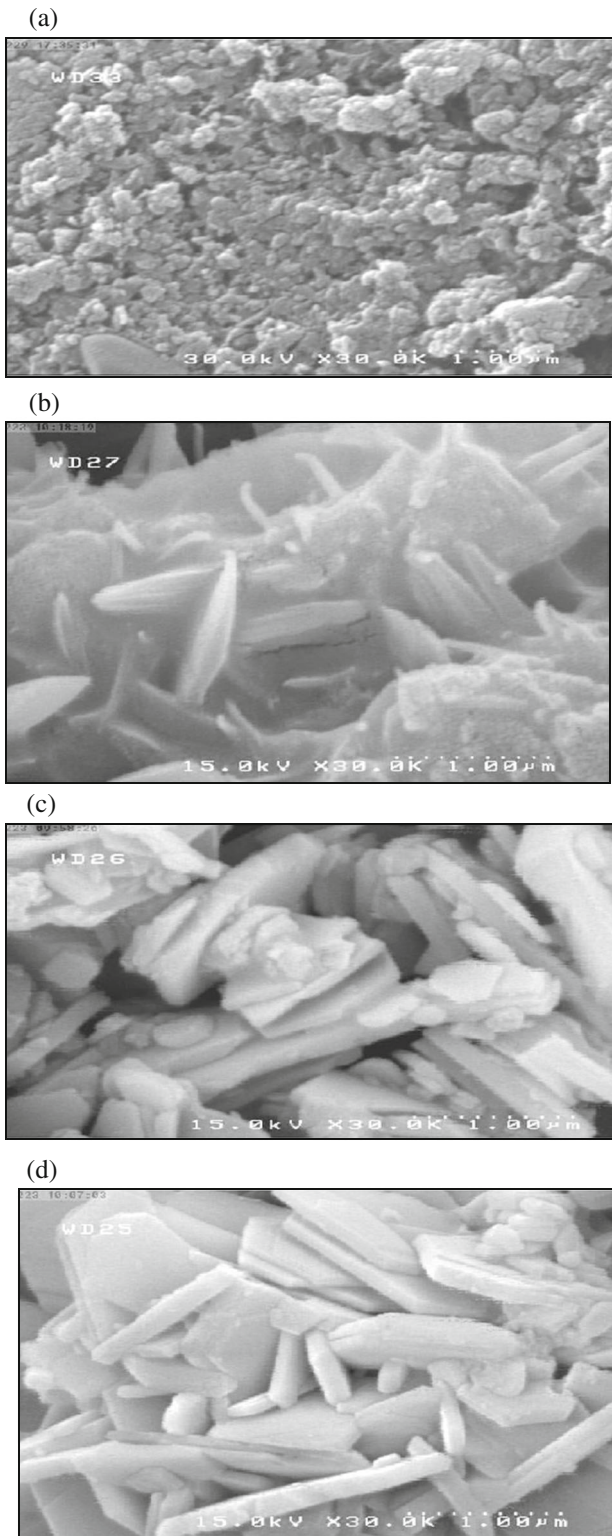
Fig. 6 SEM images of the $SrFe_{12}O_{19}$ samples: **a** blank, **b** KCl, **c** KBr, and **d** KI

(a)

(b)

Fig. 7 SEM images of the $SrFe_{11.9}Co_{0.1}O_{19}$ samples: **a** blank, and **b** KCl

the growth rate of every crystal face according to the crystal growth mechanism. The face with the rapid growth rate will gradually disappear; however, the face with slow growth

rate will be left [8]. The anion with high coordination ability is absorbed to some crystal face of $SrFe_{12-x}Co_xO_{19}$ micro-crystal to take the shielding effect. The anions of Cl^-, Br^- and I^- will influence the crystal face shielded and will have little effect on other crystal faces, making the growth rate of different crystal faces different, so the crystal will make for one dimension to form the needle-like $SrFe_{12}O_{19}$ by adding KCl. The movement of deactivator in the surface of crystal contains three phases: the deactivator in molecule is captured by the surface of crystal in the process of diffusion from environmental phase to the crystal surface, the transfer of deactivator in molecule in the crystal surface; the combination of deactivator in molecular with the steps and torsion phase. So the deactivator will take effect on the interface between the crystal phase and environmental phase. The ability of deactivator absorbed to the crystal face will directly affect the orientation growth of crystal. The easier the deactivator in molecule was absorbed, the easier crystal will grow to one dimension [8]. As for KI, it is easy to be oxidized to $K_2Fe_{10}O_{16}$ which is easy to sublime and will not be regarded as deactivator at high temperature. With the increase of the temperature, KI will get into the net structure of dried gel in melting state. KI will partly be oxidized to $K_2Fe_{10}O_{16}$. And $K_2Fe_{10}O_{16}$ will be enwrapped

(a)

(b)

(c)
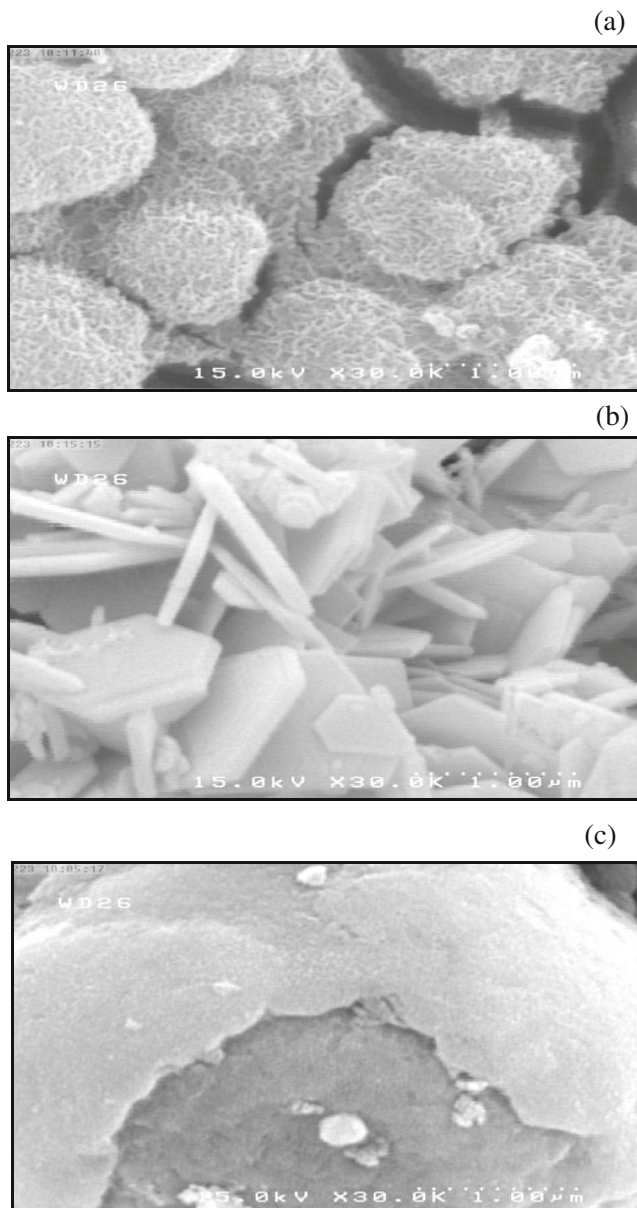
Fig. 8 SEM images of the $SrFe_{11.8}Co_{0.2}O_{19}$ samples: **a** KCl, **b** KBr, and **c** KI

by $SrFe_{12-x}Co_xO_{19}$ microcrystal generated in the process of decomposition of citric acid.

4 Conclusion

The observations from the XRD, FT-IR, and SEM studies are summarized as follows:

(i)   All of the samples of $SrFe_{12-x}Co_xO_{19}$ ($x = 0.0$, 0.1 and 0.2) without the inorganic template agents have M-type hexaferrite structure. It seems that the Fe^{3+} ions are substituted by Co^{2+} ions in the crystallography sites of the $SrFe_{12}O_{19}$ structure.

(ii)   The crystal structure of the ferrite samples does not transform and remains magnetoplumbite on the addition of inorganic template agents KCl and KBr.

(iii)   In the powder X-ray diffractographs for all the samples were obtained with KI an extra peak corresponding to the formation of $K_2Fe_{10}O_{16}$ secondary phase is observed.

(iv)   In the FT-IR spectra of all the samples, the frequency bands in the range 550–580 and 430–470 cm^{-1} correspond to the formation of tetrahedral and octahedral clusters, respectively, which confirms the presence of metal–oxygen stretching band in ferrites.

(v)   The agglomerated sample shielded along a crystal axis and hexagonal platelets have been obtained with KCl, KBr, and KI. It means that the morphology anisotropy of the samples gets increased with incorporation of KCl, KBr, and KI.

(vi)   The morphology of the sample can be easily tuned according to the research interest by incorporating with inorganic template agent.

References

1. Anis-ur-Rehman, M., Asghar, G.: Variation in structural and dielectric properties of co-precipitated nanoparticles strontium ferrites due to value of pH. Alloys Compd. **509**, 435–439 (2011)

2. Jauhar, S., Singh, J., Chandra, K., Bansal, S., Singhal, S.: Structural, morphological, magnetic and optical properties of chromium substituted strontium ferrites, $SrCr_xFe_{12-x}O_{19}$ (x=0.5, 1.0, 1.5, 2.0 and 2.5) annealed with potassium halides. Powder Technol. **212**, 193–197 (2011)

3. Iqbal M.J., Farooq, S.: Impact of Pr–Ni substitution on the electrical and magnetic properties of chemically derived nanosized strontium–barium hexaferrites. Alloys Compd. **505**, 560–567 (2010)

4. Iqbal, M.J., Ashiq, M.N.: Physical and electrical properties of Zr–Cu substituted strontium hexaferrite nanoparticles synthesized by co-precipitation method. Chem. Eng. J. **136**, 383–389. (2008)

5. Hussain, S., Shah, N.A., Maqsood, A., Ali, A., Naeem, M.: Characterization of Pb-doped Sr-ferrites at room temperature. Supercond. Nov. Magn. **24**, 1245–1248 (2011)

6. Davoodi, A., Hashemi, B.: Magnetic properties of Sn–Mg substituted strontium hexaferrite nanoparticles synthesized via coprecipitation method. Alloys Compd. **509**, 5893–5896 (2011)

7. Singhal, S., Namgyal, T., Singh, J., Chandra, K., Bansal, S.: A comparative study on the magnetic properties of $MFe_{12}O_{19}$ and $MAlFe_{11}O_{19}$ (M = Sr, Ba and Pb) hexaferrites with different morphologies. Ceram. Int. **37**, 1833–1837 (2011)

8. Yongfei, W., Qiaoling, L., Cunrui, Z., Hongxia, J.: Preparation and magnetic properties of different morphology nano- $SrFe_{12}O_{19}$ particles prepared by sol–gel method. Alloys Compd. **467**, 284 -287 (2009)

9. Ashiq, M.N., Iqbal, M.J., Gul, I.H.: Structural, magnetic and dielectric properties of Zr–Cd substituted strontium hexaferrite ($SrFe_{12}O_{19}$) nanoparticles. Alloys Compd. **487**, 341–345 (2009)

10. Iqbal, M.J., Ashiq, M.N., Gul, I.H.: Physical, electrical and dielectric properties of Ca-substituted strontium hexaferrite ($SrFe_{12}O_{19}$) nanoparticles synthesized by co-precipitation method. Magn. Magn. Mater. **322**, 1720–1726 (2010)
11. Iqbal, M.J., Farooq, S.: Enhancement of electrical resistivity of $Sr_{0.5}Ba_{0.5}Fe_{12}O_{19}$ nanomaterials by doping with lanthanum and nickel. Mater. Chem. Phys. **118**, 308–313 (2009)
12. The, G.B., Wong, Y.Ch., Tilley, R.D.: Effect of annealing temperature on the structural, photoluminescence and magnetic properties of sol–gel derived magnetoplumbite-type (M-type) hexagonal strontium ferrite. Magn. Magn. Mater. **323**, 2318–2322 (2011)
13. Tyagi, S., Baskey, H.B., Agarwala, R.C., Agarwala, V., Shami, T.C.: Development of hard/soft ferrite nanocomposite for enhanced microwave absorption. Ceram. Int. . CERI **4112**, 1–11 (2011)